INTERNATIONAL JOURNAL FOR NUMERICAL AND ANALYTICAL METHODS IN GEOMECHANICS
Int. J. Numer. Anal. Meth. Geomech., 2005; **29**:1231–1247
Published online 12 July 2005 in Wiley InterScience (www.interscience.wiley.com). DOI: 10.1002/nag.457

Coupling between anisotropic damage and permeability variation in brittle rocks

J. F. Shao[1,2,*,†], H. Zhou[2] and K. T. Chau[3]

[1] *Laboratory of Mechanics of Lille, UMR8107, CNRS, Polytech-Lille, Cité Scientifique, 59655 Villeneuve d'Ascq, France*
[2] *Institute of Rock and Soil Mechanics, The Chinese Academy of Sciences, Wuhan, China*
[3] *Department of Civil and Structural Engineering, The Hong Kong Polytechnic University, Hong Kong, China*

SUMMARY

In this paper, a coupled constitutive model is proposed for anisotropic damage and permeability variation in brittle rocks under deviatoric compressive stresses. The formulation of the model is based on experimental evidences and main physical mechanisms involved in the scale of microcracks are taken into account. The proposed model is expressed in the macroscopic framework and can be easily implemented for engineering application. The macroscopic free enthalpy of cracked solid is first determined by approximating crack distribution by a second-order damage tensor. The effective elastic properties of damaged material are then derived from the free enthalpy function. The damage evolution is related to the crack growth in multiple orientations. A pragmatic approach inspired from fracture mechanics is used for the formulation of the crack propagation criterion. Compressive stress induced crack opening is taken into account and leads to macroscopic volumetric dilatancy and permeability variation. The overall permeability tensor of cracked material is determined using a micro–macro averaging procedure. Darcy's law is used for fluid flow at the macroscopic scale whereas laminar flow is assumed at the microcrack scale. Hydraulic connectivity of cracks increases with crack growth. The proposed model is applied to the Lac du Bonnet granite. Generally, good agreement is observed between numerical simulations and experimental data. Copyright © 2005 John Wiley & Sons, Ltd.

KEY WORDS: damage models; permeability change; microcracks; induced anisotropy; brittle rocks; granite

1. INTRODUCTION

Anisotropic damage due to preferential growth and closure of microcracks subjected to non-hydrostatic stresses is the key mechanism of inelastic deformation, and leads to failure in most brittle rocks. Many experimental tests have been used to establish various mechanisms of nucleation and growth of microcracks. Under compressive stresses, sliding wing cracks seem to

*Correspondence to: J. F. Shao, Laboratory of Mechanics of Lille, UMR8107, CNRS, Polytech-Lille, Cité Scientifique, 59655 Villeneuve d'Ascq, France.
†E-mail: jian-fu.shao@polytech-lille.fr

Contract/grant sponsor: France/Hong Kong Joint Research Programme; contract/grant number: 5710QD
Contract/grant sponsor: Chinese Academy of Sciences; contract/grant number: 2004-1-7

Received 23 September 2004
Revised 20 May 2005
Accepted 24 May 2005

be the principal propagation mode of microcracks (for example, References [1–7]). Due to the roughness of crack surfaces and the grain–matrix interaction in brittle rocks, crack growth at microscopic scale normally associates with crack aperture which is the origin of macroscopic volumetric dilatancy in these materials. When the crack radius reaches some critical values, coalescence of microcracks occurs in the form of localized macrocracks and leads to the final failure of the material. The kinetics of failure is controlled by confining pressure and there is a transition from brittle failure to ductile failure when the confining pressure increases [1, 3, 8–10]. The main consequences of microcrack growth are: non-linear stress–strain relations, deterioration of elastic properties, induced anisotropy, volumetric dilatancy, irreversible strains, unilateral response due to crack closure, and hysteresis associated with frictional mechanism. These features have to be considered in the constitutive modelling. Two families of constitutive models have been developed for the description of induced damage: micromechanical approaches and phenomenological models (we do not give here an exhaustive list of models reported in the literature). The main advantage of micromechanical approaches is the ability to account for physical mechanisms involved in the nucleation and growth of microcracks. To construct a micromechanical model, two steps are generally performed. The first step consists of the evaluation of the effective elastic properties of material weakened by microcracks. The second step is to propose a suitable evolution law for microcrack growth. The main features related to microcrack growth, opening and closure, friction, interaction between cracks, could be incorporated in such micromechanical models. The macroscopic behaviour of material is then obtained through a homogenization procedure. It is generally difficult to apply these models to practical problems. Phenomenological models use internal variables to represent the density and orientation of microcracks, for instance, scalar variable for isotropic damage, second and fourth rank tensors to describe anisotropic damage. The constitutive equations are generally formulated using the concept of effective stresses based on the principle of strain energy equivalence (see Reference [11] for a comprehensive review) and from the thermodynamic potential (for example, References [12–15]). The damage evolution law is determined according to the principles of the irreversible thermodynamics. The main advantage of such models is that they provide an efficient tool for numerical modelling of engineering problems. The main weakness is that some of the concepts and parameters involved in these models are not clearly based on physical background. A number of phenomenological and micromechanical models have been successfully used in the analysis of structures made of metals, composites and concrete. However, some models have focused on the description of damage induced by tension-dominated stresses. Specific features of damage in brittle rocks induced by compressive stresses have not been properly taken into account. For example, some models are formulated by using strain-based damage criterion. Laboratory results on brittle rocks show that such a criterion could not correctly account for pressure sensitivity of such materials. Therefore, the validity of these strain-based models in the compression regime is not proven yet. This paper presents a new phenomenological model with the emphasis on the description of anisotropic damage in brittle rocks subjected to compression-dominated stresses. The basic idea is to include relevant micromechanics features in the phenomenological formalism. In addition, it is assumed that damages in brittle rocks are the prime causes of dissipation of the stored strain energy. That is, plastic deformation due to dislocation can be neglected. Macroscopic irreversible strains are related to residual opening and face mismatching of microcracks during unloading process.

In many engineering applications, rock materials are saturated with one or several phases of fluid. Therefore, coupled hydromechanical modelling of rock is essential. One key parameter in

hydromechanical modelling is the intrinsic permeability of rocks. For example, in the safety analysis of underground nuclear waste storage, the estimation of rock permeability and its evolution with induced damage is more important than the study of mechanical damage. Damage-induced permeability will change the original pore pressure distribution, which will in turn affect mechanical response of materials via poromechanical coupling. Different kinds of approaches have been proposed for the estimation of permeability in fractured media, involving empirical and statistical investigations (for example, References [16–25]). However, these investigations have been performed for a given distribution of fractures in rocks, and thus the evolutions of mechanical properties and permeability properties are normally uncoupled. There are very few studies on the coupled modelling of mechanical damage and permeability evolution. However, a lot of experimental studies have shown that there can be significant evolution of rock permeability associated with induced material damage. There is a clear correlation between volumetric dilatancy and the increase in permeability in brittle rocks. Some recent results are summarized here. For example, Oda *et al.* [23] have shown that the permeability of Inada granite at failure state in a triaxial compression test is about two to three orders of magnitude larger than that of intact granite at the same confining pressure. The maximum permeability is normally observed in the axial direction (major compressive stress). However, the anisotropy of permeability between the axial and radial directions is quite small (maximum of about 2.5). According to Schulze *et al.* [22], who conducted triaxial compressions of rock salt, the permeability was observed to increase by nearly five orders of magnitude at failure. Wang and Park [25] studied the permeability change in fine and medium sandstone, sandy mudstone and sandy shales. In these sedimentary rocks, the permeability could increase by 10 times at peak stress. Bossart *et al.* [26] investigated permeability evolution inside an excavation disturbed zone in the opalinus clay at the Mont Terri Rock Laboratory. The initial permeability of intact rock is estimated to be about 1×10^{-19} m^2. In the zone of 1.0 m around the excavated tunnel, the rock permeability varies from 1×10^{-16} to 1×10^{-13} m^2. This means that there may be substantial changes of permeability due to excavation. In Figure 1, permeability evolutions with applied deviatoric stress in triaxial compression tests are shown for two granites (data from Reference [27]). We can see that the permeability decreases in the initial stage because pre-existing cracks are progressively closed by compressive stresses and the applied deviatoric stress is not high enough (below the threshold for the onset of damage) to initiate crack growth. At the end of this stage, there may be another phase where the permeability remains nearly constant. During this phase, the initial cracks are nearly closed and the crack growth due to deviatoric stress is still negligible because opened cracks are yet to be hydraulically connected. After this stationary phase, the rock permeability increase progressively until the final failure of the sample. For the two studied granites, the rock permeability increases by two to three orders of magnitude.

Based on these experimental evidences, a fully coupled constitutive model is proposed in this paper to predict the induced damage and permeability evolution in brittle rocks. The proposed model is based on a semi-empirical and engineering-oriented approach. The mechanical damage and permeability evolution are related to microcrack growth in a consistent and unified formulation. Macroscopic volumetric dilatancy and permeability evolution are clearly attributed to stress-induced crack opening. The proposed model will be applied to a typical brittle rock; mechanical responses and permeability variations are predicted and compared with experimental data. However, the present study is limited to the mechanical behaviour of brittle rocks before the macroscopic failure, which is due to the coalescence of microcracks. The

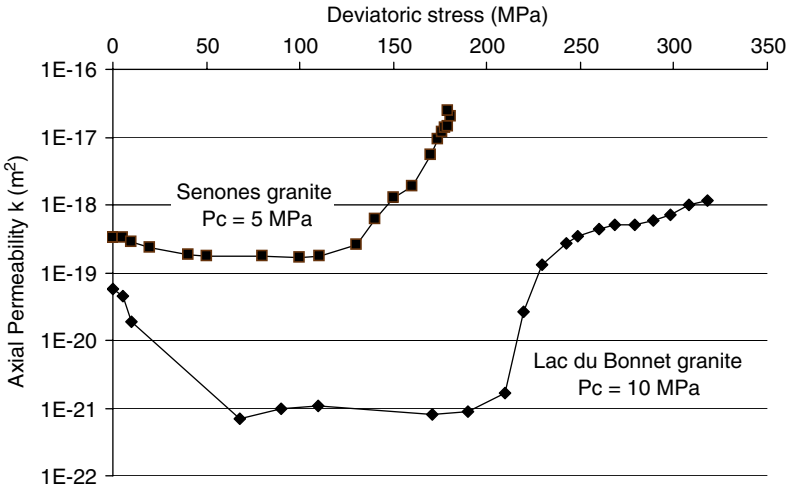

Figure 1. Variation of permeability in the axial direction during triaxial compression tests for two granites (data from Reference [27]).

mechanical response after the failure in brittle rocks is still an open topic and will be addressed in a future investigation. Further, the emphasis of this paper is to develop an engineering approach for coupling between induced anisotropic damage and permeability variation. Influences of anisotropic damage on poroelastic behaviours are then behind the topic of this paper and have been discussed in some references [28, 29].

2. ANISOTROPIC DAMAGE MODEL

It is assumed that brittle materials are subjected to compression-dominated stresses. The crack density remains small and the interaction between microcracks can be neglected before the onset of the coalescence of microcracks. The initial behaviour of materials is isotropic and anisotropy is induced by preferential growth of microcracks. Consider a representative element volume (REV) Ω containing an arbitrary distribution of microcracks in space orientation. The REV is submitted to a uniform stress field on its boundary. A continuous crack density function, denoted by $\omega(\vec{n})$, is introduced to represent orientation distribution of cracks. According to micromechanical analysis [30–32], the macroscopic free enthalpy can be obtained by the integration of crack contributions over all orientations defined on the surface of a unit sphere, denoted by S^2. This surface is decomposed into two complementary but non-overlapped sub-domains, respectively, the sub-domain S^{2+} corresponding to the orientations of opened cracks and the sub-domain S^{2-} corresponding to the orientations of closed cracks. Thus, the elastic enthalpy of cracked material is written as follows:

$$W_c = \frac{1}{2}\boldsymbol{\sigma} : \mathbb{S}^0 : \boldsymbol{\sigma} + \frac{h}{4\pi}\int_{S^{2+}} \omega(\vec{n})\left(1 - \frac{v_0}{2}\right)(\boldsymbol{\sigma}.\vec{n}).\langle \vec{n}.\boldsymbol{\sigma}.\vec{n}\rangle^{+}\vec{n}\,\mathrm{d}S$$
$$+ \frac{h}{4\pi}\int_{S^2} \omega(\vec{n})\{(\boldsymbol{\sigma}.\boldsymbol{\sigma}) : (\vec{n}\otimes\vec{n}) - \boldsymbol{\sigma} : (\vec{n}\otimes\vec{n}\otimes\vec{n}\otimes\vec{n}) : \boldsymbol{\sigma}\}\,\mathrm{d}S \quad (1)$$

where $\mathbb{S}^0$ is the initial elastic compliance tensor of the undamaged material and $\boldsymbol{\sigma}$ is the Cauchy stress tensor. The bracket $\langle \vec{n}.\boldsymbol{\sigma}.\vec{n} \rangle^+$ defines the positive cone of the normal stress in the orientation $\vec{n}$. $\omega(\vec{n})$ is the crack density in the orientation $\vec{n}$ and h the elastic compliance of crack, defined, respectively, by

$$\omega(\vec{n}) = \frac{Nr(\vec{n})^3}{\Omega}, \quad h = \frac{16(1-v_0^2)}{3E_0(2-v_0)} \tag{2}$$

In these relations, N and $r(\vec{n})$ denote the number and average radius of cracks in the orientation $\vec{n}$, respectively; and E_0 and v_0 are, respectively, Young's modulus and Poisson's ratio of the undamaged material. In order to define a state variable of anisotropic damage in the framework of macroscopic modelling, tensorial representation methods are widely used for the approximation of crack distribution [13–15, 33–35]. In the present work, the approximation with a second-order tensor is chosen as it is the simplest choice. Due to their formation history, most brittle rocks contain pre-existing microcracks, which should be taken into consideration. As an isotropic behaviour is assumed for the initial state of the material, an isotropic distribution is then considered for the initial microcracks. This should be a good approximation for isotropic rocks like granite. The macroscopic damage tensor is defined as the relative variation of crack density in each orientation:

$$\boldsymbol{D} = \frac{1}{4\pi}\int_{S^2} \omega(\vec{n})(\vec{n} \otimes \vec{n})\,\mathrm{d}S = \frac{1}{4\pi}\int_{S^2} \frac{N}{\Omega}(r(\vec{n})^3 - r_0^3)(\vec{n} \otimes \vec{n})\,\mathrm{d}S \tag{3}$$

where r_0 is the average radius of initial microcracks. By using the definition given in (3), according to the previous works by Lubarda and Krajcinovic [35], Yang *et al.* [36] and Pensee *et al.* [32], the continuous crack density function $\omega(\vec{n})$ can be expressed as a function of the macroscopic damage tensor $\boldsymbol{D}$. Therefore, for the two particular cases corresponding to solids containing fully opened and closed cracks, the macroscopic free enthalpy (1) can be analytically integrated and expressed as a function of the damage tensor $\boldsymbol{D}$:

$$W_c = \tfrac{1}{2}\boldsymbol{\sigma} : \mathbb{S}^0 : \boldsymbol{\sigma} + a_1 \operatorname{tr} \boldsymbol{D}(\operatorname{tr} \boldsymbol{\sigma})^2 + a_2 \operatorname{tr}(\boldsymbol{\sigma}.\boldsymbol{\sigma}.\boldsymbol{D}) + a_3 \operatorname{tr} \boldsymbol{\sigma} \operatorname{tr}(\boldsymbol{D}.\boldsymbol{\sigma}) + a_4 \operatorname{tr} \boldsymbol{D} \operatorname{tr}(\boldsymbol{\sigma}.\boldsymbol{\sigma}) \tag{4}$$

The four parameters a_i depend on the elastic properties of intact material as follows:

$$a_1 = \frac{-c}{70}h, \quad a_2 = \frac{7+2c}{7}h, \quad a_3 = \frac{c}{7}h, \quad a_4 = \frac{-c}{35}h \tag{5}$$

The coefficient c is equal to $c = -v_0$ for the case of opened cracks and $c = -2$ for the case of closed cracks. Note that this form of free enthalpy obtained from micromechanics consideration is similar to that proposed by Hayakawa and Murakami [12] from a fully macroscopic assumption. Further, it is important to point out that the expression of the free enthalpy given by (4) is valid only for two particular cases; all the cracks are always opened or all the cracks are always closed. The unilateral effects, related to the transition between crack opening and closure, are not taken into account. For the present study, as the material is subjected to compression-dominated stresses, we consider the case that all the cracks are closed by compressive normal stress.

For the formulation of the macroscopic anisotropic damage model, the free enthalpy function (4) is used as the thermodynamic potential, together with the second-order damage tensor $\boldsymbol{D}$, defined by (3), as the internal damage variable. Further, in most brittle rocks,

crack surfaces are not smooth and may contain asperities. Interactions between grains and matrix may generate local tensile stresses. Under compression-dominated stresses, crack face mismatch and crack opening are not uncommon during crack propagation. After unloading, a residual part of tangential sliding and normal opening is observed. On the macroscopic level, these residual sliding and opening lead to volumetric dilatancy and permanent strains after unloading. These permanent strains are not related to plastic dislocation flow but associated with damage evolution. Therefore, a damage-related inelastic strain tensor, $\boldsymbol{\varepsilon}^r(\boldsymbol{D})$, is introduced in the present model. It is not an independent state variable and its evolution is directly associated with that of damage tensor. Therefore, the damage growth is the only dissipation mechanism in the material.

By making the standard derivation of the thermodynamic potential, the stress–strain relations of the damaged material can be obtained:

$$\boldsymbol{\varepsilon} - \boldsymbol{\varepsilon}^r(\boldsymbol{D}) = \frac{\partial W_c(\boldsymbol{\sigma}, \boldsymbol{D})}{\partial \boldsymbol{\sigma}} = \frac{1+\nu_0}{E_0}\boldsymbol{\sigma} - \frac{\nu_0}{E_0}(\operatorname{tr}\boldsymbol{\sigma})\boldsymbol{\delta} + 2a_1(\operatorname{tr}\boldsymbol{D}.\operatorname{tr}\boldsymbol{\sigma})\boldsymbol{\delta} + a_2(\boldsymbol{\sigma}.\boldsymbol{D} + \boldsymbol{D}.\boldsymbol{\sigma}) + a_3[\operatorname{tr}(\boldsymbol{\sigma}.\boldsymbol{D})\boldsymbol{\delta} + (\operatorname{tr}\boldsymbol{\sigma})\boldsymbol{D}] + 2a_4(\operatorname{tr}\boldsymbol{D})\boldsymbol{\sigma} \tag{6}$$

where $\boldsymbol{\delta}$ denotes the second-order unit tensor with the components being given by the Kronecker delta function. The constitutive equations (4) can be rewritten in the following form:

$$\boldsymbol{\varepsilon} - \boldsymbol{\varepsilon}^r = \frac{\partial W_c}{\partial \boldsymbol{\sigma}} = \mathbb{S}(\boldsymbol{D}) : \boldsymbol{\sigma} \tag{7}$$

The components of the elastic compliance tensor of the damaged material, $\mathbb{S}(\boldsymbol{D})$, are given by

$$S_{ijkl}(\boldsymbol{D}) = \frac{1+\nu_0}{2E_0}(\delta_{ik}\delta_{jl} + \delta_{il}\delta_{jk}) - \frac{\nu_0}{E_0}\delta_{ij}\delta_{kl} + 2a_1(\operatorname{tr}\boldsymbol{D})\delta_{ij}\delta_{kl} + \frac{1}{2}a_2(\delta_{ik}D_{jl} + \delta_{il}D_{jk} + D_{ik}\delta_{jl} + D_{il}\delta_{jk}) + a_3(\delta_{ij}D_{kl} + D_{ij}\delta_{kl}) + a_4(\operatorname{tr}\boldsymbol{D})(\delta_{ik}\delta_{jl} + \delta_{il}\delta_{jk}) \tag{8}$$

δ_{ij} are the components the second-order unit tensor, $\boldsymbol{\delta}$.

2.1. Damage evolution and crack propagation

In the framework of thermodynamics, the damage evolution can be determined by the formulation of a dissipation potential in the space of the conjugated force associated with the damage tensor (see the reviews by Lemaitre [11] and Swoboda and Yang [15]). This kind of approach provides a rigorous framework for the definition of damage evolution law and for the verification of the fundamental inequality of damage dissipation. However, in many cases, the experimental determination of the damage evolution law is generally difficult by using the damage conjugated force, which cannot be directly measured. In rock mechanics, a more direct way may be preferred. As the damage variable is directly connected to penny shaped crack radius in different orientation, the damage evolution can be determined by the crack propagation condition based on the linear fracture mechanics. In the present model, a pragmatic approach inspired from the fracture mechanics is employed. The growth of idealized penny-shaped cracks is supposed self-similar. For each loading step, the crack radius is determined in each orientation using an appropriate crack propagation criterion. Some

experimentally based transpositions of classic results from the fracture mechanics are used for the formulation of the crack propagation criterion. The damage tensor is then calculated by the space integration according to Equation (3). For most brittle rocks, experimental data from triaxial compression tests [3, 5] have widely shown that the crack propagation condition is controlled by the confining pressure and deviatoric stress. For the set of cracks in the orientation $\vec{n}$, the normal stress applied to the crack face acts as the confining pressure and the driving force for crack propagation is the shear stress applied to the crack plane. Two modes of propagation (modes I and II) are generally combined. However, this complex propagation mode may be simplified for a phenomenological approach. The real crack may be idealized as a fictitious plane crack subjected to an equivalent normal tensile stress in an infinite body. The local tensile force, σ_t, is induced by the normal projection on the crack plane of the deviatoric stress tensor [37]. According to linear fracture mechanics, the propagation criterion of the fictitious crack may be written as $\sigma_t\sqrt{\pi r} = K_{1c}$, with r being the crack radius, σ_t the equivalent tensile stress and K_{1c} the fracture toughness. Based on the experimental evidence previously mentioned, an appropriate expression of the equivalent tensile stress is determined and the following crack propagation criterion is proposed:

$$F(\boldsymbol{\sigma}, r, \vec{n}) = \sqrt{r}\left[\sigma_n\left(\frac{f_c}{f_c + \langle -\sigma_n\rangle^+}\right)^m + f(r)\tilde{q}(\vec{n})\right] - C_{rc} \leqslant 0 \tag{9}$$

$$\sigma_n = \vec{n}.\boldsymbol{\sigma}.\vec{n}, \quad \tilde{q}(\vec{n}) = 3\langle \vec{n}.\boldsymbol{\sigma}^d.\vec{n}\rangle^+, \quad \boldsymbol{\sigma}^d = \boldsymbol{\sigma} - (\operatorname{tr}\boldsymbol{\sigma}/3)\boldsymbol{\delta} \tag{10}$$

In these equations, σ_n is the normal stress applied to the crack, and $\tilde{q}(\vec{n})$ is the normal projection of the deviatoric stress tensor. The bracket $\langle x\rangle^+$ denotes that $\langle x\rangle^+ = (x + |x|)/2$. C_{rc} is a material parameter whose physical meaning is similar to that of the fracture toughness K_{1c}. It represents the material resistance to crack propagation. The parameter m is used in order to describe non-linear dependence of crack propagation condition on the confining pressure. The uniaxial compression strength of the material is denoted by f_c; and $f(r)$ is a positive scalar-valued function controlling the kinetics of crack propagation and plays a similar role as a hardening–softening function in plastic models. The specific form of $f(r)$ can be determined from relevant experimental data on the variation of elastic properties with the evolution of damage. However, $f(r)$ must satisfy certain requirements. For small propagations of cracks, it should decrease, reflecting the relaxation of local tensile stress as the crack grows away from zone of stress concentration; as the crack length becomes long enough to interact with the nearby cracks, $f(r)$ reaches an asymptotic value. The first effect causes initially stable growth and the second marks the onset of accelerated crack interaction producing damage localization and macroscopic failure. In the present model, the following simple function having these basic features is used:

$$\begin{aligned} f(r) &= \eta\left(\frac{r_f}{r}\right), \quad r < r_f \\ f(r) &= \eta, \quad r \geqslant r_f \end{aligned} \tag{11}$$

where r_f denotes the critical crack radius for accelerated coalescence of microcracks, and η is a parameter of model. The loading–unloading condition for crack propagation in the orientation $\vec{n}$ is defined according to the Kuhn–Tucker relations [38]:

$$\dot{r} \geqslant 0, \quad F(\boldsymbol{\sigma}, r, \vec{n}) \leqslant 0, \quad \dot{r}F(\sigma, r, \vec{n}) = 0 \tag{12}$$

The proposed crack propagation criterion contains four parameters (C_{rc}, m, r_f and η), which can be related to the uniaxial compressive and tensile strengths and the curvature of failure surface in the stress space. To show this, apply the crack propagation criterion to a conventional triaxial compression test on a cylinder sample, and let the x_1 axis to be the axial orientation. Thus, the maximum of the equivalent tensile stress is obtained in the radial orientation with $\vec{n} = \vec{e}_3$. The macroscopic failure normally occurs as unstable propagation of microcracks along the axial orientation and their coalescence. By putting $\vec{n} = \vec{e}_3$ into criterion (9), the macroscopic failure criterion in triaxial compression can be determined:

$$(\sigma_3 - \sigma_1)_{\mathrm{TC}} = \frac{C_{rc}}{\eta\sqrt{r_f}} + \frac{1}{\eta}\left(\frac{f_c}{f_c - \sigma_3}\right)^m (-\sigma_3) \tag{13}$$

The uniaxial compression strength is obtained by putting $\sigma_3 = 0$:

$$f_c = \frac{C_{rc}}{\eta\sqrt{r_f}} \tag{14}$$

In the present model, the emphasis is on the damage modelling of brittle rocks under compression-dominated stresses. However, the proposed model is able to describe brittle behaviour of rocks under tensile stresses. In the case of uniaxial tensile test, the maximum of the equivalent tensile stress is obtained in the orientation $\vec{n} = \vec{e}_1$ and the macroscopic failure occurs by unstable propagation of cracks normal to the axial orientation. The uniaxial tension strength can be obtained from criterion (9) by putting $\vec{n} = \vec{e}_1$, that is:

$$f_t = \frac{C_{rc}}{(1+2\eta)\sqrt{r_f}}, \quad \frac{f_c}{f_t} = \frac{1+2\eta}{\eta} \tag{15}$$

In the case of Lac du Bonnet granite, triaxial compression tests with different confining pressures and microscopic analysis of material microstructure have been performed. For this kind of granite, the initial crack length is generally in the same order of magnitude as the average grain size. The critical crack length for coalescence is about 2–5 times of the initial length [39]. The typical values of parameters have been determined:

$$r_0 = 3 \text{ mm}, \quad r_f = 9 \text{ mm}, \quad C_{rc} = 1.03 \text{ MPa}\sqrt{\text{m}}, \quad \eta = 0.06, \quad m = 4 \tag{16}$$

With these values, the ratio between the uniaxial compression and tension strength is $f_c/f_t = 18.7$. In Figure 2, the theoretical prediction of failure stress in triaxial compression tests is shown and compared with experimental data. A good agreement is obtained. We can see that there is a strong dependency of the failure stress on the confining pressure. Obviously, for brittle rocks, the proposed non-linear criterion is more suitable than the linear functions as the classic Mohr–Coulomb criterion and that proposed by Costin [37].

2.2. Determination of damage-related irreversible strains

In the constitutive equations (6), the damage-related irreversible strain tensor, $\boldsymbol{\varepsilon}^r(\boldsymbol{D})$, is introduced in order to describe permanent strain due to residual crack opening and mismatch. The crack normal aperture can generate a macroscopic volumetric dilatancy, which is commonly observed in brittle materials. Further, the frictional shear sliding along crack surfaces can induce a macroscopic hysteretic behaviour during loading–unloading process. However, this hysteretic phenomenon is not studied in the present model and will be taken into account in a future extension of this work.

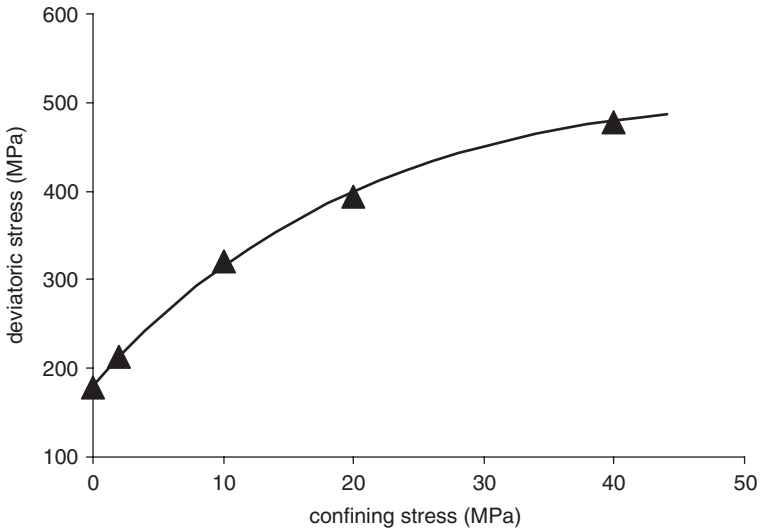

Figure 2. Comparison between the predictions of failure stress (continuous line) and experimental data in triaxial compression tests on Lac du Bonnet Granite.

Let us denote the average normal aperture, by $e(\vec{n})$ for the set of cracks in the orientation $\vec{n}$. It is assumed to be constant (in average sense) along the crack radius for a penny-shaped crack, Therefore, the tensor of damage-related irreversible strains can be determined by the integration of normal aperture over the space orientations:

$$\boldsymbol{\varepsilon}^r = \frac{1}{4\pi}\int_{S^2}\frac{N}{\Omega}e(\vec{n})(\vec{n}\otimes\vec{n})[\pi r(\vec{n})^2]\,\mathrm{d}S \tag{17}$$

Under compressive normal stress, the normal aperture of crack is due to crack face mismatch and local grain–matrix interaction during crack growth. Therefore, it is assumed that the normal crack aperture increment is proportional to the average crack radius increment, that is $\mathrm{d}e(\vec{n}) = \chi\,\mathrm{d}r(\vec{n})$, with χ being a proportionality coefficient. The value of χ can be identified from the volumetric strain dilatancy obtained in triaxial compression tests. For Lac du Bonnet granite, we have obtained $\chi = 0.005$.

3. ESTIMATION OF PERMEABILITY VARIATION

As previously mentioned, the intrinsic permeability of brittle rocks can significantly increase with growth of microcracks. In the present work, it is assumed that the rock matrix is a porous medium and microcracks are embedded in such a porous matrix. After homogenization procedure, the cracked material can be seen as an equivalent homogenized porous medium with an overall permeability tensor. The overall permeability tensor of the cracked medium is composed of two parts: the initial permeability tensor, denoted as $\mathbf{k}^0$, due to the initial porosity, and the microcrack induced permeability tensor, denoted by $\mathbf{k}^c$. The total permeability is hence $\mathbf{k} = \mathbf{k}^0 + \mathbf{k}^c$. The crack permeability is due to the crack aperture $e(\vec{n})$ and evolves with crack

growth. The average crack aperture $e(\vec{n})$ is associated with the crack radius as previously proposed. Therefore, the crack permeability directly depends on the microcrack distribution, which is determined using the crack propagation criterion presented in Section 2. As the microcrack distribution is orientation-dependent, the crack permeability tensor will be anisotropic in nature.

Consider again the representative element volume (REV) of cracked rock, composed of a porous matrix and a random distribution of microcracks, subjected to a uniform pressure gradient on the boundary. The REV can be assumed to be a homogeneous, anisotropic porous medium. The flow in the porous medium obeys Darcy's law, and the apparent fluid flow velocity $\vec{v}$ is related to the macroscopic pressure gradient ∇p through the total permeability tensor $\mathbf{k}$:

$$\vec{v} = -\frac{\mathbf{k}}{\mu}.\nabla p = -\frac{(\mathbf{k}^0 + \mathbf{k}^c)}{\mu}.\nabla p \tag{18}$$

where μ is the dynamic viscosity of fluid.

The initial rock permeability $\mathbf{k}^0$ being seen as known, the following study is now focusing on the determination of the crack permeability tensor. The crack permeability tensor $\mathbf{k}^c$ is regarded as a function of the crack orientation $\vec{n}$, the radius $r(\vec{n})$ and average aperture $e(\vec{n})$ and the number of cracks. Inside a given crack of the orientation $\vec{n}$, it is assumed that fluid flow takes place only in the direction parallel to the crack plane, and can be described by the Navier–Stokes equation for laminar flow between two parallel plates. The local flow velocity, denoted by $\vec{v}^c(\vec{n})$, is thus expressed as follows:

$$\vec{v}^c(\vec{n}) = -\frac{\lambda}{12}\frac{1}{\mu}e(\vec{n})^2(\boldsymbol{\delta} - \vec{n} \otimes \vec{n}).(\nabla p)^c, \quad 0 \leqslant \lambda \leqslant 1 \tag{19}$$

where $(\nabla p)^c$ denotes the local pressure gradient vector applied to the crack. The positive scalar λ, less than the unity, is introduced to take into account the fact that every part of a crack does not work as a conduit. But some parts may be left as dead end. When $\lambda = 1$, the classic cubic law is recovered [40]. The local pressure gradient may be related to the macroscopic gradient by an appropriate localization law [41]. In this model, we have used a simplified law by assuming that $(\nabla p)^c = \nabla p$. This implies that the local pressure gradient is equal to the macroscopic one. Therefore, the average value over the REV of local fluctuations of the pressure gradient vanishes. By analogy to the Voigt's bound of elastic compliance tensor of a cracked material, this simplification corresponds to the upper bound of crack permeability.

The macroscopic fluid flow velocity $\vec{v}$ is obtained from the averaging of local velocity field $\vec{v}^c$ over the crack volume:

$$\vec{v} = -\frac{\mathbf{k}^0}{\mu}.\nabla p + \frac{1}{\Omega}\int_\Omega \vec{v}^c \, \mathrm{d}\Omega = -\frac{\mathbf{k}^0}{\mu}.\nabla p + \frac{1}{\Omega}\int_{\Omega^c} \vec{v}^c \, \mathrm{d}\Omega^c \tag{20}$$

where Ω^c denotes the volume occupied by microcracks. After determination of the crack space distribution at a given loading step, it is easy to calculate the volume occupied by microcracks. For instance, the crack volume occupied by the set of cracks in the orientation $\vec{n}$ may be calculated by $\mathrm{d}\Omega^c(\vec{n}) = N.e(\vec{n}).\pi r(\vec{n})^2$. However, although all the cracks are contributing to macroscopic mechanical responses of a damaged rock, it is not the case for hydraulic flow. Indeed, at the local scale, a certain number of cracks may be hydraulically isolated and do not contribute to the variation of macroscopic permeability of rock. Therefore, a number of cracks

are not contributing to hydraulic flow. Let us denote the number of cracks involved in hydraulic flow by $N_h(\vec{n}) = R(\vec{n})N$, with $0 \leqslant R(\vec{n}) \leqslant 1$ being the reduction coefficient of the total number of cracks. This coefficient can be interpreted as a hydraulic connectivity coefficient of cracked rock and its value depends on the microstructure of the material. Obviously, more and more cracks are involved in macroscopic flow when microcracks grow. Therefore, the connectivity coefficient should be a function of crack radius, the following relation is proposed:

$$R(r(\vec{n})) = t_1 \left(\frac{r(\vec{n}) - r_0}{r_f - r_0} \right)^{t_2} \tag{21}$$

where t_1 and t_2 are constants to be determined. Note that r_0 and r_f are the initial and the critical crack length and have been defined in Equations (3) and (11), respectively. Introducing the crack volume and connectivity coefficient into (20), the macroscopic flow velocity can be rewritten as

$$\vec{\mathbf{v}} = -\frac{\mathbf{k}^0}{\mu}.\nabla p + \frac{N}{\Omega}\frac{1}{4\pi}\int_{S^2} R(\vec{n})\vec{v}^c(\vec{n})e(\vec{n})\pi r(\vec{n})^2 \, \mathrm{d}S \tag{22}$$

Substituting now the local flow velocity $\vec{v}^c(\vec{n})$ of (19), the macroscopic velocity of fluid is finally determined by

$$\vec{\mathbf{v}} = -\frac{\mathbf{k}^0}{\mu}.\nabla p + \left(-\frac{1}{\mu}\right)\frac{\lambda\pi}{12}\frac{N}{\Omega}\frac{1}{4\pi}\int_{S^2} R(\vec{n})e(\vec{n})^3 r(\vec{n})^2(\boldsymbol{\delta} - \vec{n} \otimes \vec{n}) \, \mathrm{d}S.\nabla p \tag{23}$$

Comparing (23) with the macroscopic Darcy law (18), the overall crack permeability tensor can be identified as follows:

$$\mathbf{k}_c = \left(\frac{N}{\Omega}\right)\left(\frac{\lambda\pi}{12}\right)\frac{1}{4\pi}\int_{S^2} R(\vec{n})e(\vec{n})^3 r(\vec{n})^2(\boldsymbol{\delta} - \vec{n} \otimes \vec{n}) \, \mathrm{d}S \tag{24}$$

4. NUMERICAL SIMULATIONS

In this section, the proposed model is applied to a typical brittle rock: the Lac du Bonnet granite. This rock has largely been studied in the context of the Underground Research Laboratory (URL) in Canada for the feasibility studies of nuclear waste storage.

According to the definition given in (3), the damage tensor is calculated by the integration over all the space orientations on the surface of a unit sphere. For the implementation of the model, the numerical integration procedure proposed by Bazant and Oh [42] is used. The components of the damage tensor are calculated by the addition of contributions from each discrete space orientation, that is

$$\boldsymbol{D} \approx \frac{2N}{\Omega}\sum_{k=1}^{N_g} w_k(r(\vec{n}_k)^3 - r_0^3)(\vec{n}_k \otimes \vec{n}_k) \tag{25}$$

where N_g denotes the number of integration points and w_k the associated weight coefficient. In a similar way, the components of the damage-related inelastic strain tensor and crack permeability tensor are respectively calculated by

$$\boldsymbol{\varepsilon}^r \approx \frac{2N}{\Omega}\sum_{k=1}^{N_g} w_k e(\vec{n}_k)(\vec{n} \otimes \vec{n})_k(\pi r(\vec{n}_k)^2) \tag{26}$$

$$\mathbf{k}_c \approx \frac{2N}{\Omega}\left(\frac{\lambda\pi}{12}\right)\sum_{k=1}^{N_g} w_k R(\vec{n}_k)e(\vec{n}_k)^3 r(\vec{n}_k)^2(\boldsymbol{\delta} - \vec{n}_k \otimes \vec{n}_k) \tag{27}$$

For the Lac du Bonnet granite, triaxial compression tests have been performed. The initial elastic parameters have been determined and the variation with confining pressure is small. The average initial elastic modulus and Poisson's ratio are: $E_0 = 68\,000$ MPa, $\nu_0 = 0.21$. The parameters involved in the damage criterion are given in the previous sections. The number of cracks per unit volume ($\Omega = 1$ m^3) is estimated to be $N = 2 \times 10^6$. The parameters involved in the hydraulic connectivity are $t_1 = 0.0001$ and $t_2 = 1$. In Figures 3–5, simulations of uniaxial compression and triaxial compression tests are presented. We can see that the numerical results agree very well with the experimental data for low- and high-confining pressures. The pressure sensitivity and volumetric dilatancy are correctly predicted.

The evolution of induced damage (tr($\boldsymbol{D}$)) with the applied deviatoric stress is shown in Figure 6 for a uniaxial compression test. The initial damage threshold depends on the average radius of initial microcracks. We can see that the damage increases non-linearly with the applied stress and the evolution rate is faster as the deviatoric stress is higher. In Figure 7, the experimental value of the cumulated number of acoustic emission counts measured during the uniaxial compression test is presented [39]. In a qualitative way, there is a good correlation between the acoustic emission counts and the predicted damage increase.

In Figure 8, the variation of permeability in the axial direction is presented for triaxial compression tests under different confining pressures. We can see that the permeability at failure state is about three orders of magnitude larger than the initial permeability of the rock. From a qualitative point of view, this result is in good agreement with the experimental data reported from various granites. Note that the Lac du Bonnet granite tested by Souley *et al.* [27] was not from the same block whereas those used in the present study are. Therefore, it is difficult to have a quantitative comparison. We can also note that the stress threshold for onset of permeability change is depending on confining pressure, which is in correlation with damage criterion. Moreover, the increase in permeability accelerates when the crack growth progresses.

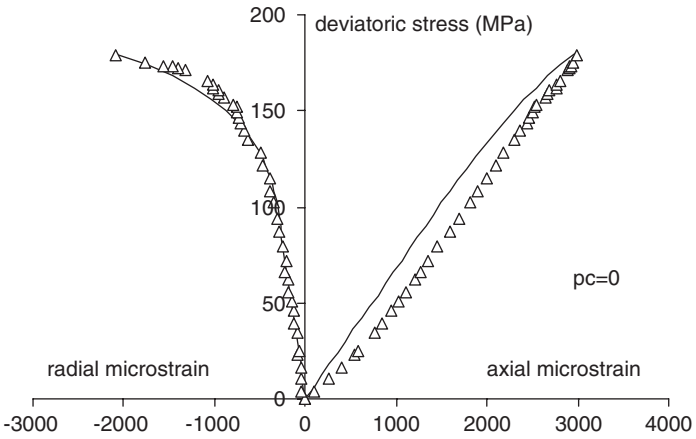

Figure 3. Simulation of a uniaxial compression test of Lac du Bonnet granite (continuous lines are numerical results).

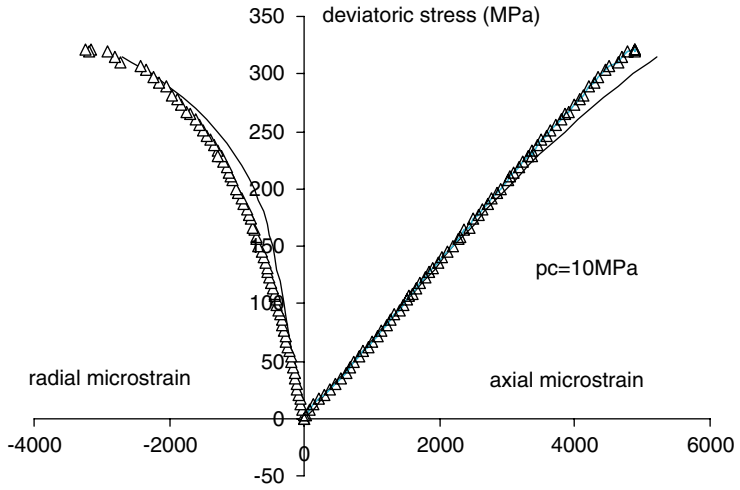

Figure 4. Simulation of a triaxial compression test of Lac du Bonnet granite with a confining pressure of 10 MPa (continuous lines are numerical results).

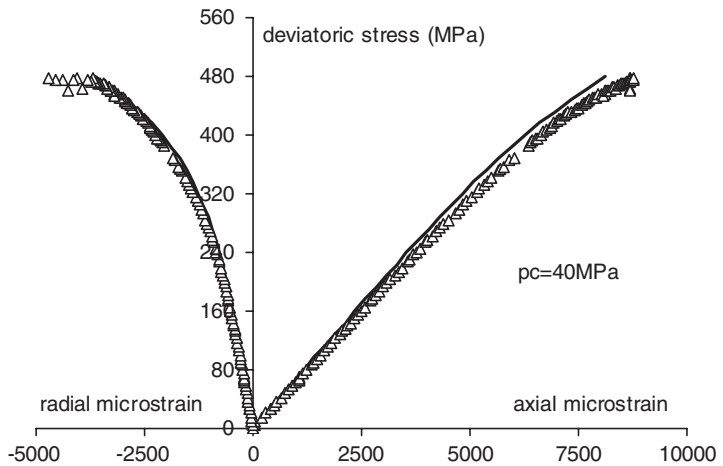

Figure 5. Simulation of a triaxial compression test of Lac du Bonnet granite with a confining pressure of 40 MPa (continuous lines are numerical results).

Figure 9 shows the permeability variation in the axial direction together with damage evolution in the radial direction during a triaxial compression test under a confining pressure of 10 MPa. Notice that in such a loading condition, the radial component of damage tensor is the major damage component while the major permeability component is in the axial direction. It is observed that the permeability change is delayed with respect to the damage evolution. That means that the hydraulic connectivity is very small during the first stage of material damage.

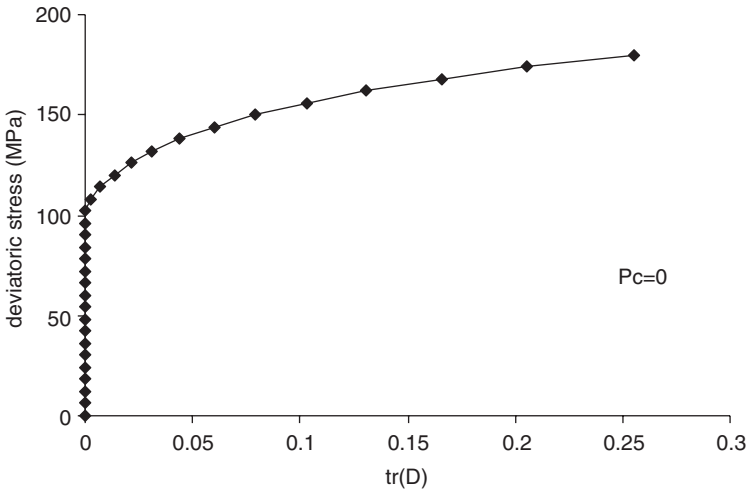

Figure 6. Evolution of damage with applied deviatoric stress in the uniaxial compression test.

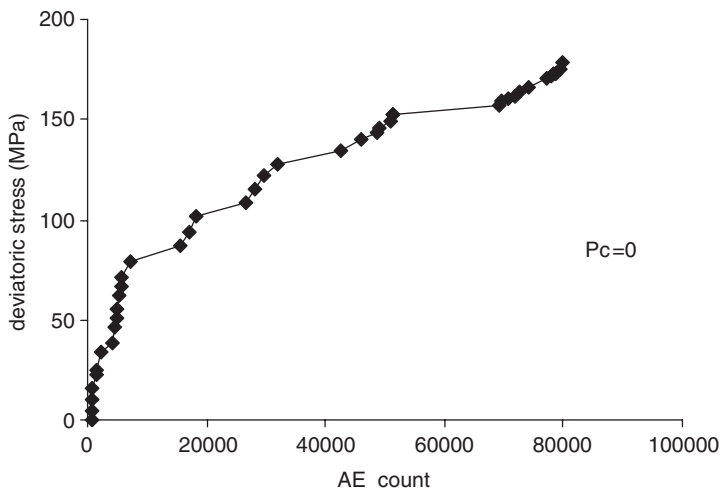

Figure 7. Evolution of acoustic emission counts with applied deviatoric stress in the uniaxial compression test.

This is also in agreement with experimental data for various granites as previously mentioned. Further, the anisotropic coefficient of permeability tensor predicted by the proposed model is about 2.0 under triaxial compression condition. This is close to the data given by Oda *et al*. [23]. Finally it is worthwhile to point out that the closure phase of initial cracks leading to the reduction of permeability is not studied in the present work and this feature will be treated in our future development.

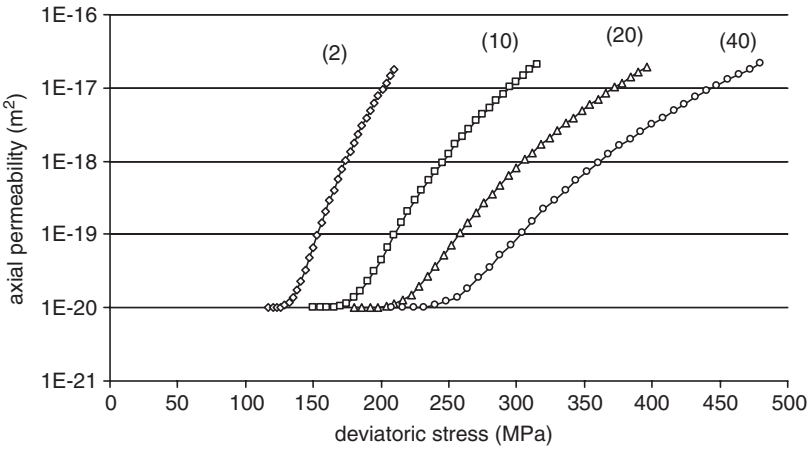

Figure 8. Variation of permeability in axial direction during various triaxial compression test on Lac du Bonnet granite (numbers in brackets indicate the confining stresses in MPa).

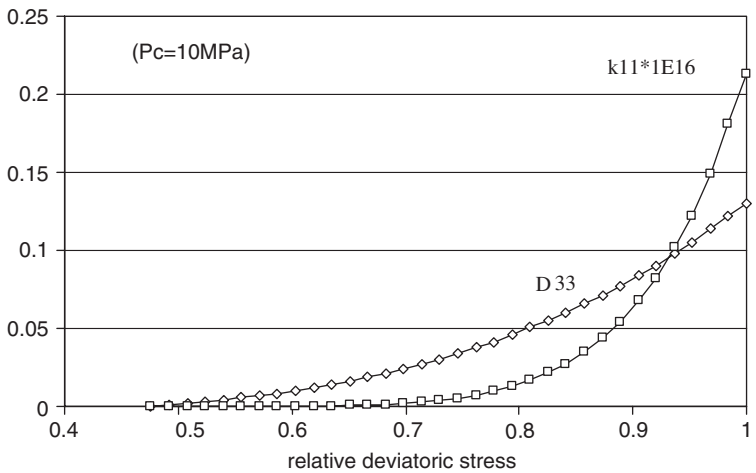

Figure 9. Variation of permeability in axial direction and growth of damage variable in radial direction during a triaxial compression test on Lac du Bonnet granite.

5. CONCLUSIONS

A coupled constitutive model is developed for induced anisotropic damage and permeability variation in brittle rocks. Based on experimental evidences, the proposed model takes into account the essential features of mechanical behaviour of brittle materials. Though a phenomenological formalism is used, the formulation of the model is based on the theoretical background of micromechanics. The effective elastic properties are deduced from the micromechanics consideration using a second-order damage tensor approximation for crack distribution. The damage evolution law is directly connected with the crack propagation

condition. A coupled formulation and unified approach is proposed to describe permeability variation together with damage growth in brittle rocks. The proposed model is applied to a typical brittle rock, the Lac du Bonnet granite. The numerical simulations are in good agreement with experimental data for both mechanical behaviour and permeability estimation. However, further validation should be conducted to check the performance of the model for more complex loading paths. In addition, our ongoing works also include the modelling of the transition from diffuse damage distribution to localized macroscopic failure in order to depict a complete picture of the failure evolution.

ACKNOWLEDGEMENTS

This work was jointly supported by a grant from the France/Hong Kong Joint Research Programme (PROCORE No. 5710QD) and the Outstanding Overseas Chinese Scholars Fund of Chinese Academy of Sciences (Reference No. 2004-1-7). The authors also thank Professors D. Kondo and L. Dormieux for helpful discussions and suggestions.

REFERENCES

1. Bieniawski ZT. Mechanism of brittle fracture of rock. *International Journal of Rock Mechanics and Mining Sciences* 1967; **4**(4):403–407.
2. Wawersik WR, Brace WF. Post-failure behavior of a granite and diabase. *Rock Mechanics* 1971: **3**:61–85.
3. Paterson S. *Experimental Deformation of Rocks*: *The Brittle Field*. Springer: Berlin, 1978.
4. Nemat-Nasser S, Horii H. Compression-induced non-planar crack extension with application to splitting, exfoliation and rock-burst. *Journal of Geophysical Research* 1982; **87**(B8):6805–6821.
5. Wong TF. Micromechanics of faulting in Westerly granite. *International Journal of Rock Mechanics and Mining Sciences* 1982; **19**:49–62.
6. Stef PS. Crack extension under compressive loading. *Engineering Fracture Mechanics* 1984; **20**(3):463–473.
7. Olsson W. Development of anisotropy in the incremental shear moduli for rock undergoing inelastic deformation. *Mechanics of Materials* 1995; **21**:231–242.
8. Fredrich JT, Evans B, Wong TF. Micromechanics of the brittle to plastic transition in Carrara marbe. *Journal of Geophysical Research* 1989; **94**:4129–4145.
9. Horii H, Nemat-Nasser S. Compression-induced microcrack growth in brittle solids: axial splitting and shear failure. *Journal of Geophysical Research* 1985; **90**(B4):3105–3125.
10. Horii H, Nemat-Nasser S. Brittle failure in compression: splitting, faulting and brittle-ductile translation. *Philosophical Transactions of the Royal Society of London* 1986; **A319**:337–374.
11. Lemaitre J. *A Course on Damage Mechanics* (2nd edn). Springer: Berlin, 1992.
12. Hayakawa K, Murakami S. Thermodynamical modeling of elastic–plastic damage and experimental validation of damage potential. *International Journal of Damage Mechanics* 1997; **6**:333–363.
13. Halm D, Dragon A. An anisotropic model of damage and frictional sliding for brittle materials. *European Journal of Mechanics – A/Solids* 1998; **17**(3):439–460.
14. Swoboda G, Yang G. An energy based damage model of geomaterials—I. Formulation and numerical results. *International Journal of Solids and Structures* 1999; **36**:1719–1734.
15. Swoboda G, Yang G. An energy based damage model of geomaterials—II. Deduction of damage evolution laws. *International Journal of Solids and Structures* 1999; **36**:1735–1755.
16. Oda M. Permeability tensor for discontinuous rock masses. *Géotecnique* 1985; **35**(4):483–495.
17. Lee CH, Deng BW, Chang JL. A continuum approach for estimating permeability for naturally fractured rocks. *Engineering Geology* 1995; **39**:71–85.
18. Zhang X, Sanderson DJ, Harkness RM, Last NC. Evaluation of the 2-D permeability tensor for fractured rock masses. *International Journal of Rock Mechanics and Mining Sciences and Geomechanics Abstracts* 1996; **33**(1):17–37.
19. Suzuki K, Oda M, Yamazaki M, Kuwahara T. Permeability changes in granite with crack growth during immersion in hot water. *International Journal of Rock Mechanics and Mining Sciences* 1998; **35**(7):907–921.
20. Chen Z, Narayan SP, Yang Z, Rahman SS. An experimental investigation of hydraulic behaviours of fractures and joints in granitic rock. *International Journal of Rock Mechanics and Mining Sciences* 2000; **37**:1061–1071.
21. Doolin DM, Mauldon M. Fracture permeability normal to bedding in layered rock masses. *International Journal of Rock Mechanics and Mining Sciences* 2001; **38**:199–210.

22. Schulze O, Popp T, Kern H. Development of damage and permeability in deforming rock salt. *Engineering Geology* 2001; **61**:163–180.
23. Oda M, Takemura T, Aoki T. Damage growth and permeability change in triaxial compression tests of Inada granite. *Mechanics of Materials* 2002; **34**:313–331.
24. Berkowitz B. Characterizing flow and transport in fractured geological media: a review. *Advances in Water Resources* 2002; **25**:861–884.
25. Wang JA, Park HD. Fluid permeability of sedimentary rocks in a complete stress–strain process. *Engineering Geology* 2002; **63**:291–300.
26. Bossart P, Meier PM, Moeri A, Trick T, Mayor JC. Geological and hydraulic characterisation of the excavation disturbed zone in the opalinus clay of the Mont Terri Rock Laboratory. *Engineering Geology* 2002; **66**:19–38.
27. Souley M, Homand F, Pepa S, Hoxha D. Damage-induced permeability changes in granite: a case example at the URL in Canada. *International Journal of Rock Mechanics and Mining Sciences* 2001; **38**:297–310.
28. Thompson M, Willis JR. A reformulation of the equations for anisotropic poroelasticity. *Journal of Applied Mechanics* (ASME) 1991; **58**:612–616.
29. Shao JF, Lu YF, Lydzba D. Damage modeling of saturated rocks in drained and undrained conditions. *Journal of Engineering Mechanics* (ASCE) 2004; **130**(6):733–740.
30. Kachanov M. Elastic solids with many cracks and related problems. In *Advances in Applied Mechanics*, vol. 30, Hutchinson J, Wu T (eds). Academic Press: New York, 1993; 259–445.
31. Nemat-Nasser S, Hori M. *Micromechanics*: *Overall Properties of Heterogeneous Materials*. North-Holland: Amsterdam, 1993.
32. Pensee V, Kondo D, Dormieux L. Micromechanical analysis of anisotropic damage in brittle materials. *Journal of Engineering Mechanics* (ASCE) 2002; **128**(8):889–897.
33. Ju JW. On energy based coupled elastoplastic damage theories: constitutive modeling and computational aspects. *International Journal of Solids and Structures* 1989; **25**(7):803–833.
34. Kachanov M. Effective elastic properties of cracked solid: critical review of some basic concepts. *Applied Mechanics Reviews* (ASME) 1992; **45**(8):304–335.
35. Lubarda VA, Krajcinovic D. Damage tensors and the crack density distribution. *International Journal of Solids and Structures* 1993; **30**(20):2859–2877.
36. Yang Q, Zhongkui L, Tham LG. An explicit expression of the second-order fabric tensor dependent elastic compliance tensor. *Mechanics Research Communications* 2001; **28**(3):255–260.
37. Costin LS. Damage mechanics in the post failure regime. *Mechanics of Materials* 1985; **4**:149–160.
38. Simo JC, Hughes TJR. *Computational Inelasticity*. Springer: New York, 1998.
39. Shao JF, Hoxha D, Bart M, Homand F, Duveau G, Souley M, Hoteit N. Modelling of induced anisotropic damage in granite. *International Journal of Rock Mechanics and Mining Sciences* 1999; **36**(8):1001–1012.
40. Snow DT. Anisotropic permeability of fractured media. *Water Resources Researches* 1969; **5**(6):1273–1289.
41. Dormieux L, Kondo D. Approche micromécanique du couplage perméabilité-endommagement. *Comptes Rendus Mécanique* 2004; **332**:135–140.
42. Bazant ZP, Oh BH. Efficient numerical integration on the surface of a sphere. *Zeitschrift fur Angewandte Mathematik und Mechanik* 1986; **66**(1):37–49.

